JGR Oceans

RESEARCH ARTICLE
10.1029/2018JC014880

Temporal and Vertical Variations of Particulate and Dissolved Optical Properties in the South China Sea

Xiaogang Xing[1], Guoqiang Qiu[2], Emmanuel Boss[3], and Haili Wang[2]

[1]State Key Laboratory of Satellite Ocean Environment Dynamics, Second Institute of Oceanography, Ministry of Natural Resources, Hangzhou, China, [2]State Key Laboratory of Marine Environmental Science, Xiamen University, Xiamen, China, [3]School of Marine Sciences, University of Maine, Orono, ME, USA

Abstract Two Bio-Argo floats measured the concentration of chlorophyll-a, the backscattering coefficient, the fluorescence of humic-like dissolved organic matter, dissolved oxygen, and temperature and salinity in the northern and central basins of the South China Sea for over 2 years. Temporal evolutions of bio-optical properties were analyzed at surface, subsurface, and in the whole water column, respectively. It was found that (1) The seasonal variability of the surface chlorophyll-a was highly controlled by photoacclimation, especially in the central basin; (2) backscattering in the upper 150 m was nearly constant, exhibiting no distinct seasonality; (3) with vertical mixing, particles from the deep chlorophyll maxima were entrained into the mixed layer resulting in enhanced surface chlorophyll during the early winter. This phenomenon may mislead a study based on satellite data which is likely to interpret it as blooming rather than a redistribution of phytoplankton within the water column; (4) analysis of a winter bloom and an anticyclonic eddy reveal that physical entrainment and biological photoacclimation modulated the vertical distributions of chlorophyll-a and particles and potentially also changes of phytoplankton community composition; and (5) fluorescent dissolved organic matter was found to be highly coupled to phytoplankton dynamics in both basins, with a maximum (after removing the contribution of physical convective mixing) located at the depth of chlorophyll-a subsurface maximum.

Key Points:
- Seasonal cycle of surface chlorophyll-a was highly modulated by photoacclimation in the South China Sea based on Bio-Argo observation
- The water column bloom started significantly later (1.5 months) than the surface bloom and was much weaker (2.5-fold vs. 15-fold)
- Both physical entrainment and photoacclimation modulated the vertical distributions of chlorophyll and backscattering in an anticyclonic eddy

Supporting Information:
- Supporting Information S1

Correspondence to:
H. Wang,
hwang@xmu.edu.cn

Citation:
Xing, X., Qiu, G., Boss, E., & Wang, H. (2019). Temporal and vertical variations of particulate and dissolved optical properties in the South China Sea. *Journal of Geophysical Research: Oceans*, *124*. https://doi.org/10.1029/2018JC014880

Received 21 DEC 2018
Accepted 25 APR 2019
Accepted article online 6 May 2019

1. Introduction

The South China Sea (SCS) is the largest tropical marginal sea in the northwestern Pacific Ocean (Figure 1), a semiclosed deep sea with two continental shelves in the northern and southwestern parts and a large deep basin in the center, connecting to the East China Sea, the Java Sea, the Pacific Ocean, and the Indian Ocean via the Taiwan Strait, the Karimata Strait, the Luzon Strait, and the Malacca Strait, respectively. The SCS is mainly forced by the alternating winter northeast and summer southwest monsoon winds, periodic typhoons, seasonal Kuroshio intrusions, and fresh water inflow (Xue et al., 2004). The circulation of the SCS is mostly driven by the monsoon winds such that the upper layer mean circulation is cyclonic in winter but anticyclonic in summer, while in the northern SCS, the circulation is also influenced by the inflows and outflows through the Taiwan and Luzon straits (Hu et al., 2000). Previous observations have shown the seasonal variation of mixed layer depth (MLD) is predominantly annual in the northern SCS, exceeding 70 m in winter and decreasing to ~ 20 m in summer (Qu et al., 2007). Wind stirring and net surface heat flux are the dominant cause of seasonal variations in MLD, with additional contributions from vertical convection and Ekman pumping (Qu et al., 2007). In winter, the enhancements of wind mixing and Kuroshio intrusion results in the deepening of MLD (Qu, 2001). In summer, the net surface heat flux is strongest due to the high solar radiation, with both wind stirring and heat-flux driven convection weakening or ceasing altogether, resulting in a very stable and shallow MLD with weakly mixing water columns (Duan et al., 2012). From the viewpoint of marine ecosystem and bio-optics, the open SCS is quite similar to deep and oligotrophic regions (Wong et al., 2007). Many studies have shown that vertical chlorophyll-a concentration is characterized by a pronounced deep chlorophyll-a maximum (DCM, also called subsurface chlorophyll maximum) at 60–100 m (Gong et al., 2014; Lu et al., 2010; Ning et al., 2004), and its seasonal cycle is associated with higher surface chlorophyll concentrations in winter and lower in summer (Gao et al., 2013; Shen et al., 2008).

Previous studies of the SCS based their analysis of upper ocean phytoplankton biomass on chlorophyll-a concentration ([Chla]) obtained from satellite observations and/or ship-based measurements and were limited in vertical and temporal scales of measurements and sensor suite used. These limitations constrain our

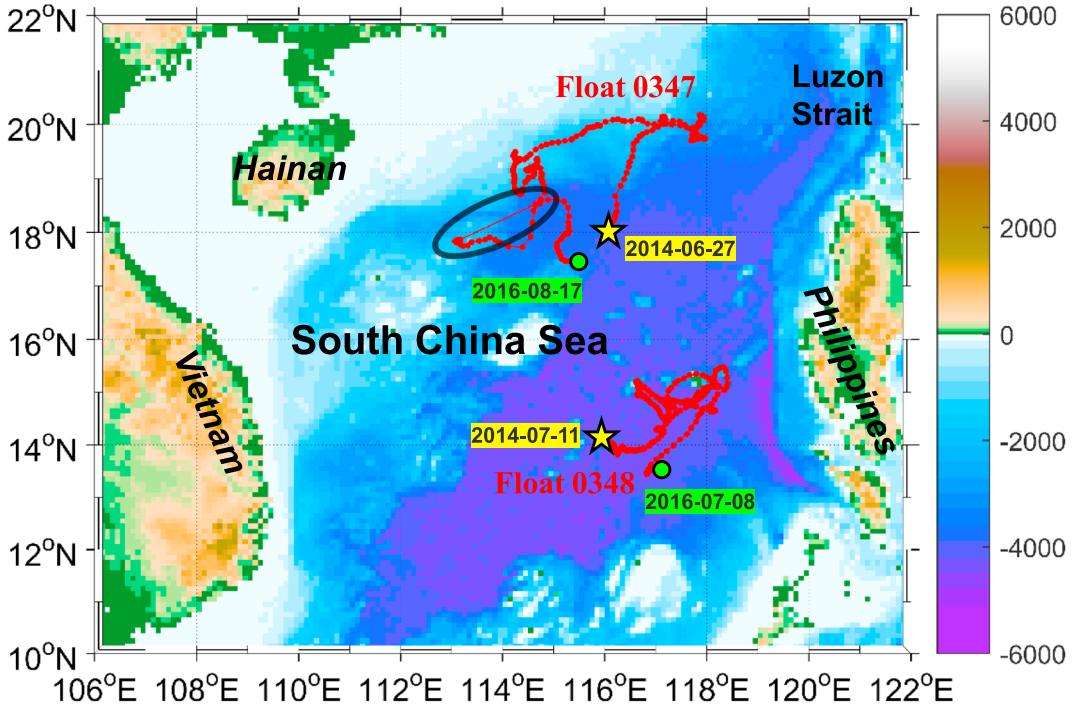

Figure 1. Trajectory map of two Bio-Argo floats (0347 and 0348) deployed in the South China Sea. The yellow stars indicate their first profiles, and green circles indicate the last ones. The black circle marks a fast shift of float position, due to a failed attempt to descend which led to an ~10-day drift at surface.

understanding of phytoplankton dynamics in SCS, considering that community composition and physiological response to light modulate [Chla] to biomass relationship and hence the interpretation of [Chla] as a biomass indicator. Particularly, photoacclimation of phytoplankton is the process whereby chlorophyll-a concentration per cell is adjusted by phytoplankton in response to the environment and their growth rate (temperature, nutrient availability, and light intensity; Geider et al., 1997), and this physiological process has been known to affect the ratio of chlorophyll-a to biomass in oligotrophic waters (Barbieux et al., 2018; Behrenfeld et al., 2005; Cullen, 1982; Siegel et al., 2005). In addition, satellite-based analysis of [Chla] in the SCS (e.g., Peñaflor et al., 2007; Shang et al., 2012; Shen et al., 2008; Tang et al., 1999; Wang et al., 2010) was limited to the near-surface layer; on the other hand, studies using in situ measured [Chla] profiles conducted during a single cruise (e.g., Chen et al., 2006; Lu et al., 2015) were not able to resolve the annual dynamics of phytoplankton nor could they account for physiological modulation of [Chla] to biomass ratio.

In the past decade, the technology and application of the autonomous profiling floats equipped with bio-optical and biogeochemical sensors has developed rapidly (Claustre et al., 2010 and ref. therein). Such floats (often called Bio- or BGC-Argo) provide novel insights into the interplay between physical processes and biological responses in the upper ocean, with particular attention given to phytoplankton blooms (Boss & Behrenfeld, 2010; Lacour et al., 2017; Mignot et al., 2018; Xing, Claustre, Uitz, et al., 2014).

The correlation between chlorophyll-a and particulate optical properties (e.g., the backscattering coefficient [b_{bp}], scattering coefficient [b_p], and beam attenuation coefficient [c_p]) have been investigated for more than 40 years, at both regional (Antoine et al., 2011; Huot et al., 2008; Kitchen & Zaneveld, 1990; Xing, Claustre, Uitz, et al., 2014) and global (Barbieux et al., 2018; Behrenfeld et al., 2005; Morel, 1988; Siegel et al., 2005, 2013) scales. Recently, b_{bp} has become the most commonly used property to study particles distribution as it can be measured in situ from a variety of platforms, for example, profiling packages (Dall'Olmo et al., 2009; Huot et al., 2008; Twardowski et al., 2001), buoy (Antoine et al., 2011), gliders (Niewiadomska et al., 2008; Thomalla et al., 2017), Bio-Argo floats (Whitmire et al., 2009; Xing, Claustre, Uitz, et al., 2014), and also retrieved from ocean color satellites (Siegel et al., 2013). While often covarying, the departures from perfect covariation between b_{bp} and [Chla] in the upper ocean provides information on regional bio-optical

characteristics (Antoine et al., 2011; Westberry et al., 2010) and/or photoacclimation processes (Behrenfeld et al., 2005) and/or the phytoplankton community composition (Cetinić et al., 2015).

In this study, we analyze data from two Bio-Argo floats which were deployed in the SCS for two years from June 2014 to August 2016, one in the northern SCS and the other in the central basin (Figure 1). A previous study (Zhang et al., 2016) analyzed the physical drivers of chlorophyll-a variability during the first year of deployment of these floats. This analysis, however, provided an incomplete view of the phytoplankton dynamics as it focused only on the surface and relied solely on the chlorophyll as a measure of phytoplankton biomass. The present study focuses on the full 2-year time series of the bio-optical fields of chlorophyll, backscattering, and fluorescent dissolved organic matter (FDOM); analyzes the likely contribution of photoacclimation to the dynamics of chlorophyll; considers the phytoplankton biomass distribution in conjunction with light and nutrient; and studies the biological responses to an anticyclonic eddy (ACE) encountered in the central basin. While our detailed results are specific to the SCS, similarities to observations in other low-latitude locations, where annual cycles in bio-optical variables have been observed, suggest our result could be generalized to other oligotrophic or subtropical locations.

2. Materials and Methods

2.1. Float-Observed Data

Two Sea-Bird Navis-BGCi floats were deployed in the northern SCS on 27 June 2014 (denoted "0347") and in the central basin (denoted "0348") on 11 July, respectively, profiling every 1 to 5 days with a vertical resolution of ~ 2 m above 1,000 m and of 50 m from 2,000 to 1,000 m depth, surfacing near local midnight to avoid the in vivo fluorescence nonphotochemical quenching (Boss et al., 2008; Cullen, 1982). The last profiles of each float were recorded on 17 August and 8 July 2016, respectively. Float 0348 kept its position within the central basin, within a radius of ~120 km, and has conducted 241 profiles; 0347 moved first toward the north during the first 6 months of its mission, observing a strong winter bloom close to the Luzon Strait, and then drifted westward along with the Kuroshio intrusion current during the subsequent 6 months. Subsequently it drifted to the south, with a trajectory spanning 5° of longitude and 2.5° of latitude (Figure 1), performing 245 profiles during its 2-year lifetime.

Both floats were equipped with a SBE 41CP CTD, a SBE 63 dissolved oxygen probe (DO; μmol/kg), and a WETLabs MCOMS 3-in-1 optical sensor which included sensors for chlorophyll-a fluorescence ([Chla]; mg/m^3), FDOM (ppb), and particulate backscattering coefficient at 700 nm (b_{bp} [700]; m^{-1}; see Table 1). Near the float deployment times and locations, water was collected for in situ calibration of the float's chlorophyll-a fluorometer (analyzed using high-performance liquid chromatography; Ras et al., 2008) and as a check for the DO data using the Winkler wet-chemical method (Winkler, 1888).

2.2. Ancillary Data

For our analysis, we use the daily multisatellite blended wind speed (SSW; m/s; ftp://eclipse.ncdc.noaa.gov/pub/seawinds/) provided by National Oceanic and Atmospheric Administration's *National Centers for Environmental Information*, daily photosynthetically available radiation at the surface (PAR0; mol quanta·m^{-2}·day^{-1}; https://oceancolor.gsfc.nasa.gov/l3/) provided by NASA, and daily sea level anomaly (SLA; m; ftp://ftp.aviso.altimetry.fr) provided by Archiving, Validation and Interpretation of Satellite Oceanographic (AVISO) (see Table 1 for acronym definitions and notation).

2.3. Derived Data

In our analysis, [Chla] and DO profiles are smoothed using a five-point median filter, while FDOM and b_{bp} are smoothed with a seven-point median filter, due to the higher variability observed in these signals.

Potential density is derived from pressure, temperature, and salinity based on the Thermodynamic Equation Of Seawater-2010 (TEOS-10, McDougall & Barker, 2011); MLD is estimated based on a threshold potential density difference (0.03 kg/m^3) from a near-surface value (at 10 m).

The averaged values of [Chla] and b_{bp} within MLD are denoted as the $[Chla]_{ML}$ and b_{bpML}, respectively. DCM is defined as a subsurface depth where [Chla] is the maximum of the profile, and is larger than the averaged [Chla] within the ML by 10%. For analysis, we separate the upper water column into three layers within which we integrate [Chla] and b_{bp}. "ML" denotes the mixed layer, spanning from surface to MLD;

Table 1
Symbols Used in This Study

Symbol	Definition	Unit	Source/derivation
b_{bp}	particulate backscattering coefficient at 700 nm	m^{-1}	Bio-Argo observation
b_{bpDCM}	b_{bp} at z_{DCM}	m^{-1}	z_{DCM} and b_{bp}
b_{bpML}	averaged b_{bp} from 0 m to MLD	m^{-1}	MLD and b_{bp}
[Chla]	chlorophyll-a concentration	mg/m^3	Bio-Argo observation
[Chla]/b_{bp}	Ratio of [Chla] and b_{bp}	mg/m^2	[Chla] and b_{bp}
$[Chla]_{DCM}$	[Chla] at z_{DCM}	mg/m^3	z_{DCM} and [Chla]
$[Chla]_{ML}$	averaged [Chla] from 0 m to MLD	mg/m^3	MLD and [Chla]
dFDOM	biology-related FDOM	ppb	*T*, *S*, FDOM
$dFDOM_{YSM}$	dFDOM at z_{YSM}	ppb	*T*, *S*, FDOM
DO	dissolved oxygen concentration	μmol/kg	Bio-Argo observation
FDOM	fluorescent dissolved organic matter	ppb	Bio-Argo observation
K_d (PAR)	downward diffused attenuation coefficient of PAR	m^{-1}	[Chla] and model
MLD	mixed layer depth	m	σ
PAR	daily PAR profile	mol quanta·m^{-2}·day^{-1}	K_d (PAR) and PAR0
PAR_{DCM}	daily PAR at z_{DCM}	mol quanta·m^{-2}·day^{-1}	z_{DCM} and PAR
PAR_{ML}	median daily PAR within the mixed layer, that is, PAR(z = MLD/2)	mol quanta·m^{-2}·day^{-1}	MLD and PAR
PAR0	daily photosynthetically available radiation at surface	mol quanta·m^{-2}·day^{-1}	NASA
S	practical salinity	‰	Bio-Argo observation
SLA	daily sea level anomaly	m	reanalysis AVISO
SSW	daily blended sea surface wind speed	m/s	NECI/NOAA
T	temperature	°C	Bio-Argo observation
z_{DCM}	depth of deep chlorophyll maximum	m	[Chla]
z_{NO3}	depth of CANYON-derived NO_3 concentration as 2 μmol/kg	m	*T*, *S*, DO and CANYON model
z_{T22}	thermocline depth of *T* as 22 °C	m	*T*
z_{YSM}	Depth of maximum dFDOM	m	*T*, *S*, FDOM
$z_{0.415}$	isolume depth of daily PAR as 0.415 μmol quanta·m^{-2}·day^{-1}	m	PAR
σ	potential density	kg/m^3	*T*, *S* and *P*
$\sum b_{bpML}$	integrated b_{bp} from 0 m to MLD	/	MLD and b_{bp}
$\sum b_{bpSub}$	integrated b_{bp} from MLD to 150 m	/	MLD and b_{bp}
$\sum b_{bp150}$	integrated b_{bp} from 0 to 150 m	/	b_{bp}
$\sum[Chla]_{ML}$	integrated [Chla] from 0 m to MLD	mg/m^2	MLD and [Chla]
$\sum[Chla]_{Sub}$	integrated [Chla] from MLD to 150 m	mg/m^2	MLD and [Chla]
$\sum[Chla]_{150}$	integrated [Chla] from 0 to 150 m	mg/m^2	[Chla]

"Sub" means the subsurface layer, spanning from MLD to 150 m (below which no chlorophyll is observed within our data set); and "150" spanning from surface to 150 m, representing the whole layer where phytoplankton are significant.

Several light-related variables are derived from PAR0 and [Chla]. First, the diffused attenuation coefficient of Photosynthetically Active Radiation (PAR) (K_d [PAR]) profile is modeled from [Chla], through two empirical relationships of Morel et al. (2007); equations (1) and (2). Then, the daily PAR profile is estimated based on PAR0 and K_d (PAR;1 equation (3). Further, the PAR vertical distribution is used for the estimation of (i) the median light intensity within mixed layer PAR_{ML} (i.e., PAR at MLD/2, following Behrenfeld et al., 2005), (ii) the light intensity at the DCM (PAR_{DCM}), and (iii) the depth of the 0.415-mol quanta·m^{-2}·day^{-1} isolume, which was found by Letelier et al. (2004) in oligotrophic northeastern Pacific to be the depth of the base of the DCM and was utilized by Boss and Behrenfeld (2010) as an index for the euphotic layer.

$$K_d(490) = 0.0166 + 0.0825Chla^{0.6529} \quad (1)$$

$$K_d(\mathrm{PAR}) = 0.0864 + 0.884\,K_d(490)\text{-}0.00137\,K_d(490)^{-1} \quad (2)$$

$$\mathrm{PAR}(z) = \mathrm{PAR0}\times\exp\left(-\int_0^z K_d(\mathrm{PAR},z)\mathrm{d}z\right) \quad (3)$$

As there were no nitrate sensors on the floats, two depth values are derived as the proxy for the nitracline: (i) the 22 °C isotherm (z_{T22}) which was used by Zhang et al. (2016) as the proxy for nutricline and could be expected to covary with the depth where $[NO]_3$ reaches 0–5 μmol/kg in SCS based on a regional empirical

relationship (Chen et al., 2006); and (ii) the depth which the neural-network model CANYON finds $[NO_3]$ = 2 μmol/kg (z_{NO3}; Sauzède et al., 2017). CANYON estimates $[NO_3]$ based on the date, location, temperature, salinity, and dissolved oxygen. Note that CANYON was trained without any data from the SCS, thus, the estimated z_{NO3} used here is only for reference.

dFDOM was calculated as the difference between FDOM and a FDOM model based on a multiple linear relationship (MLR) with both temperature and salinity (Carlson et al., 2010), formulated as

$$\mathrm{FDOM} = \alpha_1 + \alpha_2 \times T + \alpha_3 \times S + \mathrm{dFDOM} \tag{4}$$

For each float data, first we solve a multiple linear regression of FDOM versus T and S (equation (4)) without considering dFDOM and then apply the regressed coefficients (i.e., α_1, α_2, and α_3) to equation (4) to calculate the residual between FDOM and ($\alpha_1 + \alpha_2 \times T + \alpha_3 \times S$) to obtain dFDOM. Since ($\alpha_1 + \alpha_2 \times T + \alpha_3 \times S$) represents the part explained by physical processes (when computed in the layer below the MLD), dFDOM can be regarded as production/loss part by biogeichemical processes, including photo-oxidation at surface and production from phytoplankton, zooplankton, and/or bacterial activities. The maximum dFDOM is identified as the yellow substance subsurface maximum (YSM); the depth of YSM is denoted as z_{YSM}.

3. Results and Discussion

The temporal (June 2014 to August 2016) and vertical variations in the upper layer (0–200 m) of T, S, [Chla], b_{bp}, O_2, FDOM, and derived dFDOM are plotted in Figure 2. In this study, the evolution of the physical fields are analyzed first (section 3.1 followed by the seasonal evolution of [Chla] and b_{bp} in the upper ocean (sections 3.2 to 3.5). In addition, the biological responses to two events are discussed, the winter bloom in the northern basin and an ACE encountered in the central basin (Figure 2 and section 3.6). Finally, coupling between FDOM and phytoplankton is expounded upon (section 3.7).

3.1. Physical Setting

The surface light intensity (PAR0) was higher in summer and lower in winter, modulated by clouds in addition to the solar cycle (Figures 3a and 4a). The MLD (Figures 3b and 4b) deepened in winter and shoaled in the summer, with the deepest MLD reaching 100 m in the northern SCS, consistent with previous studies (Duan et al., 2012; Qu et al., 2007). The averaged MLD was 27–28 m for both floats, with the northern float (0347) observing deeper ML in winter and shallower ML in summer, compared to the central basin one (0348). Isotherm z_{T22} generally followed the dynamics of MLD for both floats, except for an obvious uplift in the first winter (December 2014 to March 2015) which suggested the presence of upwelling near the Luzon Strait as reported previously (Chen et al., 2006; Lu et al., 2015). Sea surface winds (SSW) displayed the monsoon's features, with stronger winds in winter and summer (Figures 3a and 4a). MLD was correlated to SSW (r = 0.66 and 0.61 in the northern and central SCS, respectively).

PAR_{ML} correlates similarly to PAR0 and MLD, suggesting that the light intensity in ML is similarly affected by the surface light and mixing, which is expected based on its definition. Besides, we found that $z_{0.415}$ was driven by PAR0, as the former is proportional to the logarithm of the latter and the integrated distribution of [Chla], with little response to changes in MLD; nitracline z_{NO3} and isotherm z_{T22} were correlated to SLA, with r = 0.33 and 0.53 in the northern basin, and r = 0.53 and 0.77 in the central basin, respectively. This indicates that mesoscale processes (e.g., eddies) likely affect the thermocline as well as nutricline, which in turn had a biological response (see section 3.6.2).

3.2. Chlorophyll-a and Particles at DCM

Generally, in the northern SCS, the DCM appeared in spring after the MLD shoaling, deepened in summer with increasing solar illumination (PAR0), shoaled in the autumn, and disappeared in winter due to strong mixing (Zhang et al., 2016). This evolution is typical of oligotrophic regions such as the North Pacific subtropical gyre and Mediterranean Sea (Letelier et al., 2004; Mignot et al., 2014), with, however, shallower MLD in the SCS. In the central basin, the DCM was present throughout the year at ~70 m with very limited seasonal variation, exhibiting similar characteristics as those of ultra-oligotrophic waters such as in the South Pacific subtropical gyre. Although the DCM in South Pacific subtropical gyre could reach more than 150 m (Mignot et al., 2014), the reasons for the permanent DCM are the same: (i) high sunlight supporting a DCM at depth,

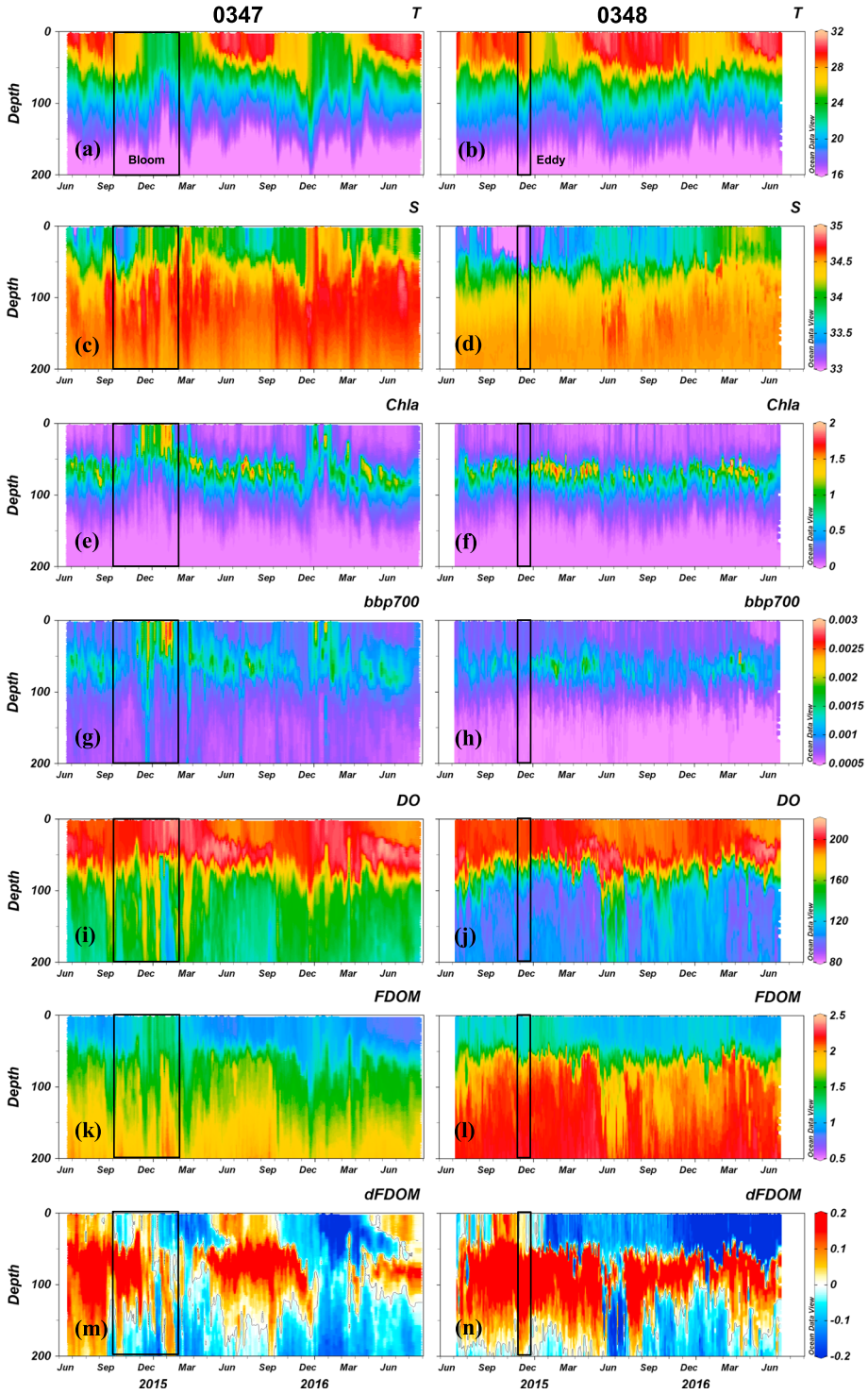

Figure 2. Time series of temperature (a and b), salinity (c and d), [Chla] (e and f), b_{bp} (g and h), DO (i and j), FDOM (k and l), and dFDOM (m and n) observed by two Bio-Argo floats (0347 and 0348). The black rectangles represent the winter bloom period (left) and an eddy event (right) analyzed in section 3.6. dFDOM = biology-related FDOM; DO = dissolved oxygen; FDOM = fluorescent dissolved organic matter.

(ii) low nutrient maintaining a low surface chlorophyll concentration (and hence a relatively low attenuation of light in the water), and (iii) relatively weak mixing which deepens the ML in the winter but not sufficiently to erode the DCM layer.

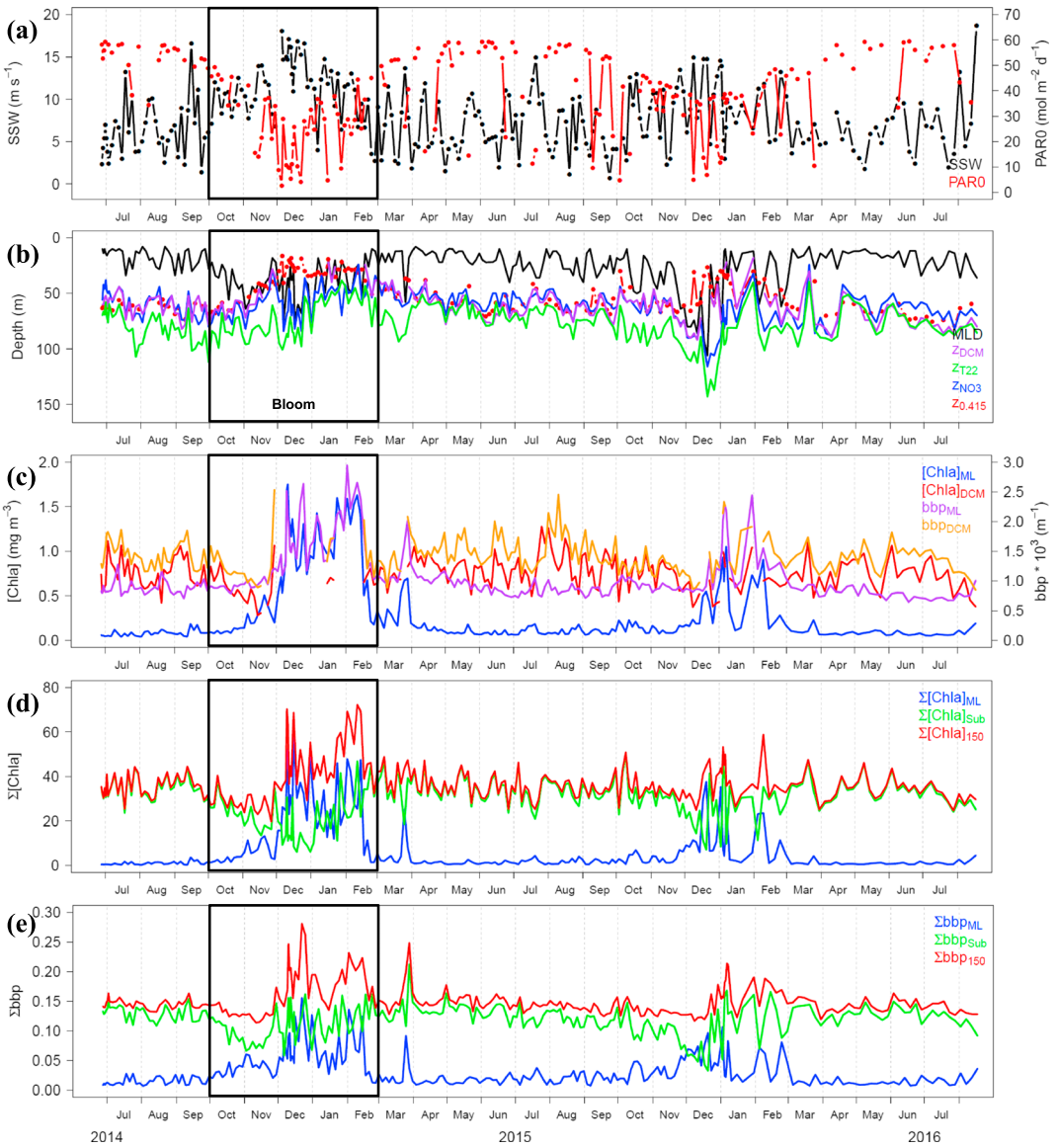

Figure 3. Time series of (a) SSW and PAR0; (b) MLD, z_{DCM}, z_{T22}, z_{NO3}, and $z_{0.415}$; (c) $[Chla]_{ML}$, $[Chla]_{DCM}$, b_{bpML}, and b_{bpDCM}; (d) $\sum[Chla]_{ML}$, $\sum[Chla]_{Sub}$, and $\sum[Chla]_{150}$; and (e) $\sum b_{bpML}$, $\sum b_{bpSub}$, and $\sum b_{bp150}$ observed by Float 0347. The black rectangle represents the winter bloom period. MLD = mixed layer depth; PAR0 = photosynthetically available radiation at the surface; SSW = sea surface winds.

For both floats, the estimated nitracline z_{NO3} and isolume $z_{0.415}$ correlated with z_{DCM}, with the correlation of 0.58 and 0.71 in the northern SCS and of 0.47 and 0.84 in the central basin, respectively (Tables 2 and 3). The light-driven patterns of chlorophyll and nitrate are similar to those in oligotrophic waters (Letelier et al., 2004) and are consistent with 1-D steady state modeling (Fennel & Boss, 2003; Gong et al., 2017).

$[Chla]_{DCM}$ had a relatively high correlation with PAR_{ML} in both basins ($r = 0.54$ and 0.49 for the northern and central one, respectively), and with z_{NO3} in the central basin ($r = -0.52$), but b_{bpDCM} has no significant correlation with any physical properties. This means that the chlorophyll-a concentration and phytoplankton biomass (as inferred from backscattering; e.g., Graff et al., 2015) were not simply coupled.

3.3. Chlorophyll-a and Particles at Surface

At the surface of northern SCS, both biological properties ($[Chla]_{ML}$ and b_{bpML}) displayed similar seasonality, higher in winter and lower in summer (Figure 3c). Especially in the winter of 2014–2015, Float 0347 observed a strong winter bloom close to Luzon Strait (see section 3.6.1).

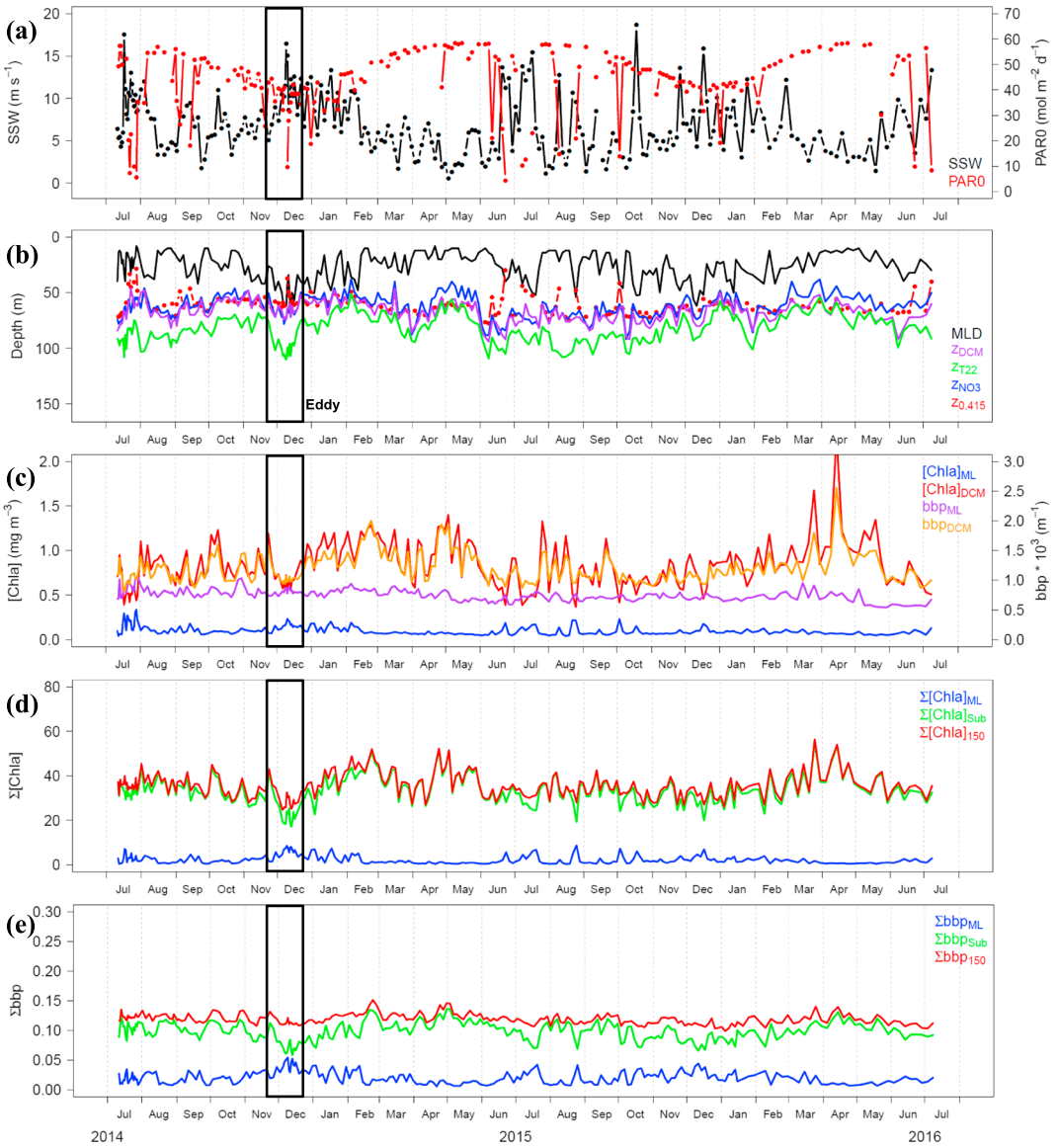

Figure 4. Same as Figure 3, but for Float 0348. The black rectangle represents an eddy event.

In the northern SCS, both $[Chla]_{ML}$ and b_{bpML}, as well as their ratio, had a higher correlation with $z_{0.415}$ than any other physical variable (Table 2), implying the light-driven pattern was also related to the surface [Chla]. In fact, the variability of [Chla] and b_{bp} at the surface in the northern SCS were more related to the light intensity than to SSW or mixing (MLD).

In the central basin, both biological properties had a very weak seasonal cycle at the surface (Figure 4c). $[Chla]_{ML}$ was highly correlated with PAR_{ML} ($r = 0.80$), but b_{bpML} had no correlation with any physical property, similar to other ultra-oligotrophic waters where photoacclimation dominates the seasonal cycles of [Chla], and the phytoplankton biomass (b_{bp} as its proxy) displays weak seasonality (Barbieux et al., 2018; Behrenfeld et al., 2005; Mignot et al., 2014). Consistent with photoacclimation, a high correlation was found between $([Chla]/b_{bp})_{ML}$ and PAR_{ML} ($r = -0.87$; see section 3.5).

3.4. Depth-Integrated Chlorophyll-a and Particles

In the northern SCS, integrated values at surface and subsurface were highly coupled with the variability of MLD and PAR_{ML}, while the total inventories ($\sum[Chla]_{150}$ and $\sum b_{bp150}$) were more correlated to $z_{0.415}$ (Tables 2 and 3). In the central basin, MLD played an important role in distribution phytoplankton

Table 2
Correlation Coefficient (r) Between Bio-optical Properties and Physical Properties

r	SSW	MLD	ln (PAR0)	ln (PAR_{ML})	$z_{0.415}$	z_{T22}	z_{NO3}	SLA
$[Chla]_{ML}$	0.48*	0.33*	−0.49*	−0.66*	**−0.83***	−0.14	−0.10	−0.26*
b_{bpML}	0.32*	0.17	−0.34*	−0.46*	**−0.75***	−0.22*	−0.18	−0.39*
$([Chla]/b_{bp})_{ML}$	0.59*	0.47*	−0.62*	−0.79*	**−0.87***	−0.01	0.00	−0.15
z_{DCM}	−0.02	0.29*	0.19	0.04	**0.71***	0.46*	0.58*	0.33*
$[Chla]_{DCM}$	−0.46*	−0.45*	0.41*	**0.54***	0.18	−0.37*	−0.33*	−0.23*
b_{bpDCM}	−0.36*	−0.45*	0.26	0.38*	−0.12	−0.33*	−0.25*	−0.36*
$\sum[Chla]_{ML}$	0.60*	0.62*	−0.52*	**−0.85***	−0.76*	0.05	0.09	−0.12
$\sum b_{bpML}$	0.66*	0.82*	−0.52*	**−0.89***	−0.67*	0.19	0.23*	−0.03
$\sum[Chla]_{Sub}$	−0.66*	−0.72*	0.55*	**0.79***	0.49*	−0.18	−0.24*	−0.11
$\sum b_{bpSub}$	−0.52*	**−0.83***	0.35*	0.61*	0.14	−0.40*	−0.37*	−0.35*
$\sum[Chla]_{150}$	0.10	0.06	−0.14	−0.34*	**−0.52***	−0.13	−0.13	−0.28*
$\sum b_{bp150}$	0.18	0.02	−0.21	−0.34*	**−0.56***	−0.20	−0.14	−0.39*

Note. Bold value represents the highest *r* for each biological property and $r \geq 0.5$; the asterisks (*) represent statistically significant values ($p < 0.001$). MLD = mixed layer depth; PAR0 = photosynthetically available radiation at the surface; SSW = sea surface winds.

biomass (using b_{bp} as the proxy) between surface and subsurface, while PAR_{ML} were more correlated to [Chla] distribution. $\sum[Chla]_{150}$ and $\sum b_{bp150}$ had very limited variability, especially $\sum b_{bp150}$. This implies that the variability of MLD had no effect on the total biomass change within the whole water column, consistent with the central SCS being a very stable system with strong coupling between phytoplankton growth and loss terms. Most of the variability in [Chla] in this region is driven as a physiological response to changing light levels during the seasonal cycle.

3.5. Correlation Between Chlorophyll-a and Particulate Backscattering

Our data regarding the relationship of [Chla] and b_{bp} is consistent with the global relationship derived by Barbieux et al. (2018), at both ML and DCM (Figure 5a). The difference of scatter points between ML and DCM as well as the discrepancy of two regressed relationships suggest that there was less [Chla] per unit of b_{bp} at the surface compared to the subsurface, owing to either photoacclimation process (Behrenfeld et al., 2005) or/and the phytoplankton community composition (Cetinić et al., 2015).

Phytoplankton cells lower their intracellular Chla in response to the high-light conditions, which is most obvious in surface waters of oligotrophic subtropical gyres (Kitchen & Zaneveld, 1990). If this process is important in the nutrient-depleted and high-light environment of the central SCS, we would expect the $[Chla]/b_{bp}$ ratio, a proxy of the ratio of chlorophyll to phytoplankton biomass to be inversely correlated to

Table 3
Same as Table 2, but for Float 0348

r	SSW	MLD	ln (PAR0)	ln (PAR_{ML})	$z_{0.415}$	z_{T22}	z_{NO3}	SLA
$[Chla]_{ML}$	0.66*	0.42*	−0.69*	**−0.80***	−0.80*	0.15	−0.02	0.18
b_{bpML}	0.27*	0.07	−0.19	−0.18	−0.44*	−0.06	−0.19	−0.01
$([Chla]/b_{bp})_{ML}$	0.70*	0.50*	−0.74*	**−0.87***	−0.78*	0.19	0.03	0.20
z_{DCM}	−0.17	0.01	0.06	0.07	0.47*	0.63*	**0.84***	0.38*
$[Chla]_{DCM}$	−0.39*	−0.33*	0.45*	0.49*	0.20	−0.51*	**−0.52***	−0.41*
b_{bpDCM}	−0.34*	−0.35*	0.32*	0.42*	0.08	**−0.50***	−0.50*	−0.37*
$\sum[Chla]_{ML}$	0.73*	0.85*	−0.49*	**−0.89***	−0.50*	0.25*	0.10	0.28*
$\sum b_{bpML}$	0.64*	**0.97***	−0.29*	−0.80*	−0.28*	0.19	0.10	0.20
$\sum[Chla]_{Sub}$	−0.37*	−0.57*	0.32*	**0.58***	0.09	−0.40*	−0.44*	−0.42*
$\sum b_{bpSub}$	−0.58*	**−0.90***	0.29*	0.75*	0.17	−0.24*	−0.20	−0.22*
$\sum[Chla]_{150}$	−0.18	−0.36*	0.20	0.37*	−0.07	−0.37*	−0.47*	−0.39*
$\sum b_{bp150}$	−0.26*	−0.44*	0.19	0.40*	−0.02	−0.20	−0.25*	−0.15

Note. Bold value represents the highest *r* for each biological property and $r \geq 0.5$; the asterisks (*) represent statistically significant values ($p < 0.001$). MLD = mixed layer depth; PAR0 = photosynthetically available radiation at the surface; SSW = sea surface winds.

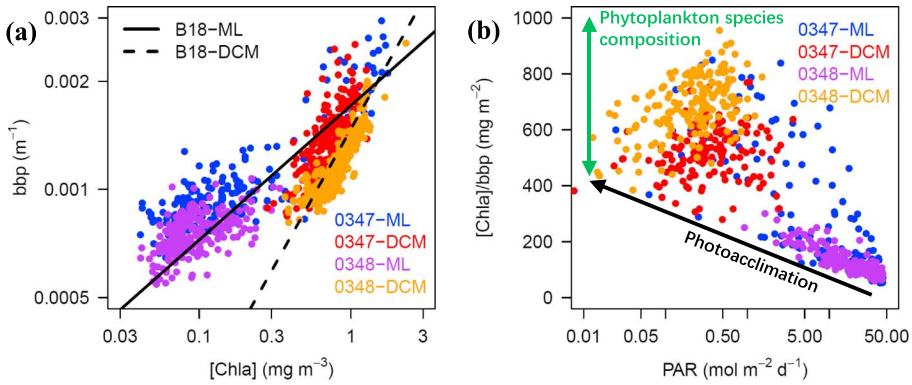

Figure 5. Scatter plots between [Chla] and b_{bp} (a), and between PAR and [Chla]/b_{bp} (b). "0347-ML" and "0347-DCM" represent the averaged value in the mixed layer and at the DCM observed by Float 0347, respectively (with similar notation for Float 0348). "B18-ML" and "B18-DCM" represent the regression relationships of Barbieux et al. (2018) based on a global Bio-Argo data set in mixed layer (ML) and at DCM, respectively. DCM = deep chlorophyll-a maximum.

light. Indeed, our observation by Float 0348 showed a high correlation between $[Chla]_{ML}$ and PAR_{ML} ($r = -0.72$) and between $([Chla]/b_{bp})_{ML}$ and PAR_{ML} ($r = -0.78$).

On the other hand, although b_{bp} is often used as a proxy for particulate organic carbon or even phytoplankton carbon (C_{phy}; Behrenfeld et al., 2005; Boss & Behrenfeld, 2010; Graff et al., 2015; Mignot et al., 2018; Thomalla et al., 2017), its variability also depends on other aspects (e.g., particle size distribution, shape, structure, and refractive index; e.g., Stramski et al., 2004), thus sensitive to picophytoplankton (Cetinić et al., 2015) or highly refractive algae (e.g., cocolithophore, Balch et al., 1996), as well as to nonalgal particles (e.g., detritus, bacteria, and viruses, Ahn et al., 1992, Loisel et al., 2001). Cetinić et al. (2015) proposed using the ratio of [Chla] and b_{bp} as a particle size index. In situ measurements in SCS discovered that picophytoplankton (*Prochlorococcus*) dominated at surface in summer, but nanophytoplankton (mainly haptophytes) and microphytoplankton (mainly diatoms) dominated in winter (Xiao et al., 2018). Thus, we may expect, for a given light level, to see relatively larger b_{bp} for a given [Chla] in the low-[Chla] range, as shown in Figure 5a.

A scatter plot of the ratio [Chla]/b_{bp} as function of PAR (Figure 5b), within the ML as well as the DCM, reveals that for values of PAR > 5 μmol m^{-2} day^{-1} [Chla]/b_{bp} changes in a tight and opposite relation with light, consistent with photoacclimation. For lower PAR values, there was not a tight relationship. This could indicate that in these low and weakly varying PAR levels species composition was a stronger driver of [Chla]/b_{bp}. It is noteworthy that the observation that $([Chla]/b_{bp})_{DCM}$ had a weak and positive correlation with PAR_{DCM} was also found in oligotrophic gyres and Mediterranean Sea (Barbieux et al., 2018, see their Figure 7d) and was interpreted as being representative of the presence of large phytoplankton.

Our data showed the two processes as two dimensions of [Chla]/b_{bp} variability and suggest that (i) community composition variability dominated [Chla]/b_{bp} at DCM, where light level was relatively constant (note, however, that at low PAR uncertainties in its value are relatively high as it is computed from an extrapolation from the surface [equation (4)]); (ii) photoacclimation process dominated $([Chla]/b_{bp})_{ML}$ in the central basin; and (iii) both processes affected the dynamics of $([Chla]/b_{bp})_{ML}$ in the northern SCS. Hence, [Chla]-b_{bp} relationship with regard to light level provides an important diagnostic to investigate the biological and physiological responses to physical processes (see also Lacour et al., 2015).

3.6. Event Analysis

In this section, two specific events in the SCS, a winter bloom and an ACE, observed by 0347 and 0348, respectively, are discussed in detail.

3.6.1. Winter Bloom

The continuous observations of the vertical variations provided by profiling floats allow us to build a 2-D (depth-time) view of upper-ocean [Chla], b_{bp}, FDOM, oxygen, as well as physical properties during the winter of 2014–2015. Float 0347 recorded concurrent MLD deepening from early October 2014 and an

enhancement of surface [Chla] ($[Chla]_{ML} > 0.1$ mg/m^3, Figure 3c), consistent with studies based on remotely sensed satellite data (also see Zhang et al., 2016). This "surface bloom" attained its peak (maximal $[Chla]_{ML}$ reached 1.75 mg/m^3, a 15-fold increase in magnitude) in December, was sustained for about 2.5 months and was followed by a fast decay in February, with $[Chla]_{ML}$ attaining low values (< 0.1 mg/m^3) at the end of May.

b_{bpML} exhibited an analogous evolution as that of [Chla], except that in mid-December it had high values below the MLD (Figure 2g). The transient high values in the deeper layer could be associated with particulate matter deposited from the upper layer, similarly to those observed in the North Atlantic bloom by Briggs et al. (2011), though here several events were observed. Although b_{bp} had the similar pattern to [Chla] during the winter bloom, it was enhanced about 2.5-fold (from 0.001 to 0.0025 m^{-1}). The difference between the [Chla] and b_{bp} in accumulation (15-fold compared to 2.5-fold) is consistent with a strong photoacclimation response to decreasing in situ PAR and suggests this bloom was about 6 times smaller in phytoplankton biomass than suggested by the change in [Chla]. FDOM increased with depth with high values in the ML (Figure 2k), and dFDOM showed a loss of FDOM at the same time. It is consistent with FDOM being entrained from below the ML to surface and photo-oxidized within the ML.

The depth-integrated [Chla] and b_{bp} indicated that phytoplankton accumulation (e.g., bloom) for the whole water column started from the end of November (Figures 3d and 3e). During the first 2 months of surface bloom (October and November), both $\sum[Chla]_{150}$ and $\sum b_{bp150}$ exhibited a slight decrease. This means that the surface increase was due to entrainment of particles from the stratified DCM layer into the mixed layer. During the same period, the total phytoplankton biomass decreased slightly (Figure 2a). In fact, the "water column bloom" (defined as a sustained increase in phytoplankton biomass) lasted only 3 months, significantly shorter than the surface bloom (5 months in total). Although the entrainment process was sometimes considered in previous studies on SCS winter bloom (e.g., Wang et al., 2010), it was difficult to identify it accurately due to lack of vertical observation. The same process also appeared in November and December 2015, when a smaller winter bloom was recorded by Float 0347 during its second year.

Both $\sum[Chla]_{150}$ and $\sum b_{bp150}$ indicated that phytoplankton biomass changed by about 1.75-fold during the bloom period (Figures 3d and 3e), implying that using surface variability significantly overestimates the phytoplankton bloom magnitude ($[Chla]_{ML}$ varied by 15-fold). It also suggests that satellite-based studies on the bloom in tropical and subtropical areas, where a DCM exists, likely suffer from this issue.

3.6.2. ACE

It has been demonstrated that Bio-Argo float is helpful in documenting eddy-induced biological responses (e.g., Alkire et al., 2012; Boss et al., 2008; Dufois et al., 2017; Llort et al., 2018), especially with their added vertical scale.

A strong ACE with >20-cm difference of SLA (Figure 6a) was captured by Float 0348 in the central SCS, from November to December 2014 (see Figure S1 in the supporting information). During this period, MLD deepened due to the eddy pumping effect (McGillicuddy, 2016), and the isotherm z_{T22} was depressed as well (Figure 6b). Affected by this, DCM and the nitracline z_{NO3} deepened. However, no collocated change of $z_{0.415}$ was observed. Both [Chla] and b_{bp} at the DCM were reduced by ~60% and ~30%, respectively (Figure 6d), while both [Chla] and b_{bp} at surface had a slight increase (Figure 6d). $\sum[Chla]_{ML}$ and $\sum b_{bpML}$ also slightly increased, in contrast with depressed $\sum[Chla]_{Sub}$ and $\sum b_{bpSub}$ and for the whole phytoplankton active layer ($\sum[Chla]_{150}$ and $\sum b_{bp150}$; Figures 6c and 6e), which is consistent with entrainment of nutrients into the mixed layer during this period. The surface increase of [Chla] was larger than b_{bp}, together with the high correlation between $([Chla]/b_{bp})_{ML}$ and PAR_{ML}, implying significant photoacclimation (Figure 6).

In an ACE in the south Indian subtropical gyre, Dufois et al. (2017) found larger particles in mixed layer of the eddy center than outside and suggested that the entrainment process stirred the DCM layer phytoplankton into ML, and thus its mixed-layer community composition in the eddy center was similar to the DCM population depth outside of eddy. Unfortunately, we did not have an independent index of particle size, but we do observe a DCM with higher $[Chla]/b_{bp}$ than ML for a given PAR (Figure 5b).

As for the DCM depth, a decreased ($[Chla]/b_{bp}$) was observed from eddy edge to center, that was correlated with PAR_{DCM}. As discussed above, the Chla-b_{bp} relationship at the DCM may be more related to community

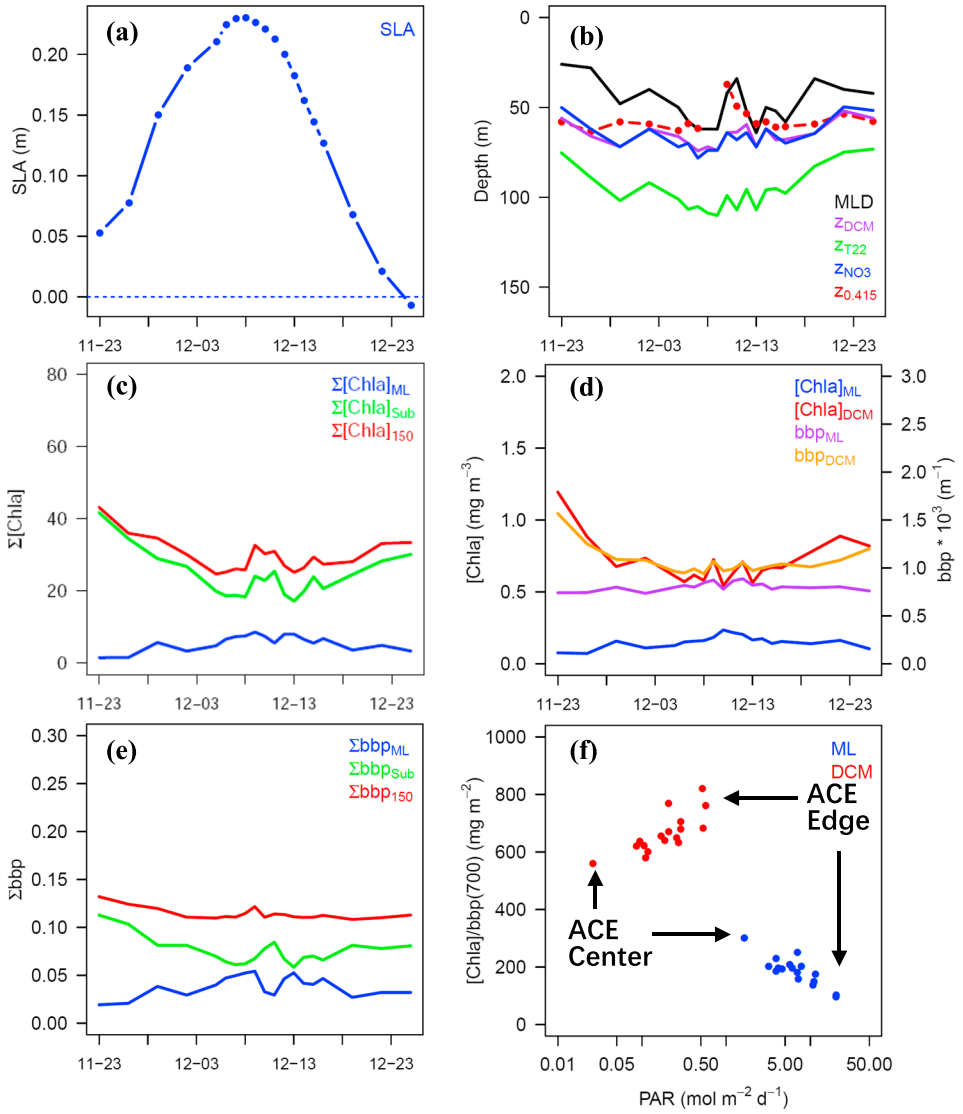

Figure 6. An anticyclonic eddy encountered by Float 0348 from November to December of 2014: Time series of (a) SLA; (b) MLD, z_{DCM}, z_{T22}, z_{NO3}, and $z_{0.415}$; (c) $\sum[Chla]_{ML}$, $\sum[Chla]_{Sub}$, and $\sum[Chla]_{150}$; (d) $[Chla]_{ML}$, $[Chla]_{DCM}$, b_{bpML}, and b_{bpDCM}; (e) $\sum b_{bpML}$, $\sum b_{bpSub}$, and $\sum b_{bp150}$; and (f) the scatter plot between $[Chla]/b_{bp}$ and PAR in the mixed layer (ML) and at DCM, respectively. MLD = mixed layer depth; SLA = sea level anomaly.

composition variability. For example, it may indicate more picophytoplankton at the DCM than outside. The phytoplankton community response to eddies have been studied with in situ data (e.g., Coria-Monter et al., 2014; Huang et al., 2010; Liang et al., 2018; Vaillancourt et al., 2003), and models (e.g., Laiolo et al., 2016; Xiu & Chai, 2011). In particular, both Huang et al. (2010) and Liang et al. (2018) reported that ACEs in the SCS have a decreasing contribution of diatoms at the subsurface while an increasing contribution of picophytoplankton (*Synechococcus* and *Prochlorococcus*) compared to outside the eddies. A biological model simulated a similar response and concluded that ACE limited the diatom growth relative to outside due to decrease in silicate in the euphotic zone due to eddy pumping (Xiu & Chai, 2011).

3.7. Relationship of FDOM and Chlorophyll-a Distribution

The MLR analysis on FDOM and *T*/*S* resulted in two relationships which represent the part of FDOM which may be explained by physical conservative mixing when conditions are stratified. The dFDOM calculated as the residual between FDOM and MLR, for the two floats was

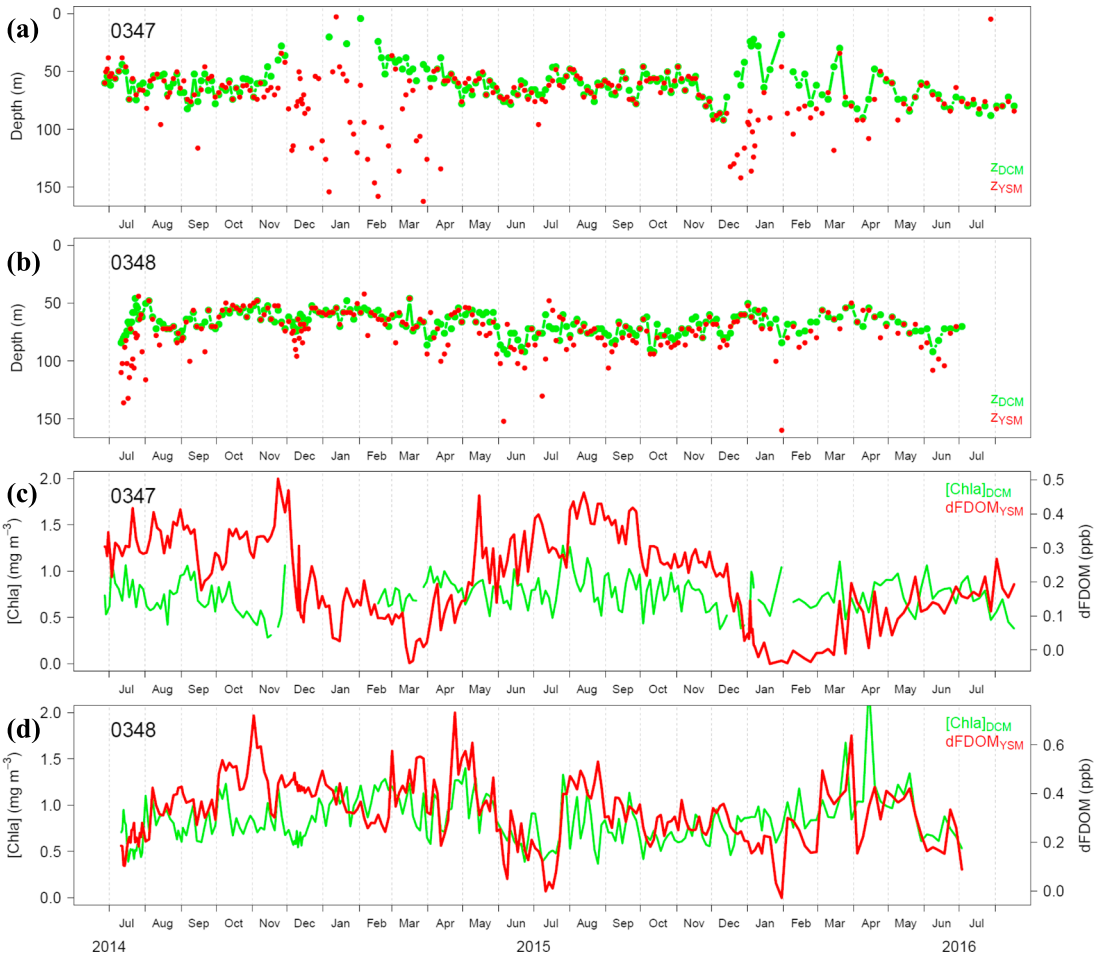

Figure 7. Time series of z_{DCM} and z_{YSM} (a and b), and [Chla] at DCM ([Chla]$_{DCM}$) and dFDOM at YSM (dFDOM$_{YSM}$) (c and d) observed by Float 0347 (a and c) and 0348 (b and d), respectively. DCM = deep chlorophyll-a maximum; dFDOM = biology-related FDOM; FDOM = fluorescence by dissolved organic matter.

$$\mathrm{dFDOM} = \mathrm{FDOM} - (7.867 - 0.079 \times T - 0.1376 \times S) \tag{5}$$

$$\mathrm{dFDOM} = \mathrm{FDOM} - (-2.252 - 0.064 \times T + 0.1585 \times S) \tag{6}$$

Here it is worthy to note that α_1 (7.867 for 0347 and −2.252 for 0348) also includes the dark currents of the CDOM fluorometer (e.g., Xing et al., 2012). Besides, the difference of α_2 and α_3 between two equations is likely due to different water masses encountered by two floats in the northern and central basins, respectively.

FDOM in the SCS increased monotonously with depth (Figures 2k and 2l). However, dFDOM exhibited a subsurface maximum (see (Figures 2m and 2n). The depth of this subsurface maximum z_{YSM} is highly correlated to z_{DCM} in the central basin (Figure 7b), and also in the northern SCS, except for the winter-spring period (Figure 7a). This phenomenon was observed in the Mediterranean Sea (Xing, Claustre, Wang, et al., 2014) and suggests that FDOM was biologically controlled, either directly produced by phytoplankton (exudates; Fukuzaki et al., 2014; Romera-Castillo et al., 2010) or via phytoplankton-affected bacterial activity (Rochelle-Newall & Fisher, 2002; Kinsey et al., 2018). The decoupling (winter-spring) only appeared in the northern basin where winter mixing was strong and the DCM eroded, with a weak YSM (dFDOM <0.2 ppb, Figure 7c); in the spring, the coupling was rebuilt after the subsurface waters restratified, and FDOM began to accumulate from March. Comparatively, z_{YSM} and z_{DCM} were always coupled in the central basin (Figure 7a), where the system was stable all the year round.

As for the YSM magnitude ($dFDOM_{YSM}$), it displayed a clearer seasonality in the northern basin, with an increase in magnitude from spring to summer, and a decline from autumn to winter, but there was neither apparent correlation between $[Chla]_{DCM}$ and $dFDOM_{YSM}$ (Figures 7c and 7d), nor obvious time lag effect which could explain the temporal difference between FDOM enhancement and phytoplankton bloom (3- to 5-month time lag found in the Mediterranean Sea; Xing, Claustre, Wang, et al., 2014). In the central basin, the seasonal variation of maximum dFDOM (i.e., YSM magnitude) was less remarkable. This is consistent with a very stable system where biogeochemical processes are near steady state. In addition, the YSM thickness (~60–100 m in Figures 2m and 2n, where black curves represent the contour of dFDOM = 0) in SCS was 2 times wider than the DCM layer (~40 m), consistent with particulate settling and degradation causing an FDOM max at and below the DCM (Figures 7a and 7b).

4. Conclusions

Thanks to the high resolution (~2 m, 1 to 5 days) and long-term (~2 years) observations obtained with two bio-optical profiling floats, the dynamic of bio-optical variables in the SCS in general and phytoplankton in particular were revealed. While they are consistent with past studies regarding the surface dynamics of [Chla], they enable us to better understand both the surface dynamics as well as those within the whole euphotic layer.

Our key findings are as follows:

1. Surface variability of chlorophyll-a at seasonal scale was found to be highly modulated by the photoacclimation process, especially in the central basin, where all bio-optical properties were nearly constant and most of the observed variability could be explained based on seasonal changes in light.
2. The DCM followed the $z_{0.415}$ isolume and the nitracline well, similar to what was found in oligotrophic waters elsewhere (Letelier et al., 2004) and from the 1-D model (Gong et al., 2017).
3. The mixing-induced entrainment played an important role in the vertical redistribution of particles, especially during the winter bloom period in the northern SCS. Analysis of whole water column properties suggest that the water column bloom started significantly later (~1.5 months) than the "surface" bloom observed by satellite. As a result of photoacclimation, [Chla] displays a much larger change (15-fold) than backscattering (~2.5-fold), implying that previous studies, based only on [Chla], overestimated the bloom magnitude.
4. Both the physical entrainment and photoacclimation were found to modulate the vertical distributions of chlorophyll-a and particles in an ACE, in addition to indication to changes of phytoplankton community composition;
5. After removing the part of FDOM that linearly correlates to the physical fields (i.e., dFDOM), FDOM was found to have its maximum at the same depth of DCM in both basins, except the winter-spring period in the northern basin, implying a tight link between FDOM and phytoplankton in the euphotic layer, similar to observations in the Mediterranean Sea (Xing, Claustre, Wang, et al., 2014). It supports the assumption that phytoplankton and their associated ecosystem are directly related to FDOM dynamics.

Acknowledgments
This paper represents a contribution to the National Key Research and Development Program of China (2016YFA0601101), Scientific Research Fund of the Second Institute of Oceanography, SOA, China (QNYC1702 and 14283), the National Natural Science Foundation of China (41876032, 41576100, and 41076114), the scientific research fund of Qingdao National Laboratory for Marine Science and Technology (QNLM2016ORP0103), and the National Basic Research Program of China (2015CB954002). The Bio-Argo data used were obtained from the Xiamen University (https://odc.xmu.edu.cn/BioArgo/DataBin/0347_databin.txt and https://odc.xmu.edu.cn/BioArgo/DataBin/0348_databin.txt).

References

Ahn, Y.-H., Bricaud, A., & Morel, A. (1992). Light backscattering efficiency and related properties of some phytoplankters. *Deep Sea Research Part A. Oceanographic Research Papers*, *39*(11-12), 1835–1855. https://doi.org/10.1016/0198-0149(92)90002-B

Alkire, M. B., D'Asaro, E., Lee, C., Perry, M. J., Gray, A., Cetinić, I., et al. (2012). Estimates of net community production and export using high-resolution, Lagrangian measurements of O_2, NO_3^-, and POC through the evolution of a spring diatom bloom in the North Atlantic. *Deep Sea Research Part I: Oceanographic Research Papers*, *64*, 157–174. https://doi.org/10.1016/j.dsr.2012.01.012

Antoine, D., Siegel, D. A., Kostadinov, T., Maritorena, S., Nelson, N. B., Gentili, B., et al. (2011). Variability in optical particle backscattering in contrasting bio-optical oceanic regimes. *Limnology and Oceanography*, *56*(3), 955–973. https://doi.org/10.4319/lo.2011.56.3.0955

Balch, W. M., Kilpatrick, K. A., Holligan, P., Harbour, D., & Fernandez, E. (1996). The 1991 coccolithophore bloom in the central North Atlantic. II. Relating optics to coccolith concentration. *Limnology and Oceanography*, *41*(8), 1684–1696. https://doi.org/10.4319/lo.1996.41.8.1684

Barbieux, M., Uitz, J., Bricaud, A., Organelli, E., Poteau, A., Schmechtig, C., et al. (2018). Assessing the variability in the relationship between the particulate backscattering coefficient and the chlorophyll a concentration from a global Biogeochemical-Argo database. *Journal of Geophysical Research: Oceans*, *123*, 1229–1250. https://doi.org/10.1002/2017JC013030

Behrenfeld, M. J., Boss, E., Siegel, D. A., & Shea, D. M. (2005). Carbon-based ocean productivity and phytoplankton physiology from space. *Global Biogeochemical Cycles*, *19*, GB1006. https://doi.org/10.1029/2004GB002299

Boss, E., & Behrenfeld, M. (2010). In situ evaluation of the initiation of the North Atlantic phytoplankton bloom. *Geophysical Research Letters*, *37*, L18603. https://doi.org/10.1029/2010GL044174

Boss, E., Swift, D., Taylor, L., Brickley, P., Zaneveld, R., Riser, S., et al. (2008). Observations of pigment and particle distributions in the western North Atlantic from an autonomous float and ocean color satellite. *Limnology and Oceanography*, *53*(5), 2112–2122. https://doi.org/10.4319/lo.2008.53.5_part_2.2112

Briggs, N., Perry, M. J., Cetinić, I., Lee, C., D'Asaro, E., Gray, A. M., & Rehm, E. (2011). High-resolution observations of aggregate flux during a sub-polar North Atlantic spring bloom. *Deep Sea Research Part I: Oceanographic Research Papers*, *58*(10), 1031–1039. https://doi.org/10.1016/j.dsr.2011.07.007

Carlson, C. A., Hansell, D. A., Nelson, N. B., Siegel, D. A., Smethie, W. M., Khatiwala, S., et al. (2010). Dissolved organic carbon export and subsequent remineralization in the mesopelagic and bathypelagic realms of the North Atlantic basin. *Deep-Sea Research Part II: Topical Studies in Oceanography*, *57*(16), 1433–1445. https://doi.org/10.1016/j.dsr2.2010.02.013

Cetinić, I., Perry, M. J., D'Asaro, E., Briggs, N., Poulton, N., Sieracki, M. E., & Lee, C. M. (2015). A simple optical index shows spatial and temporal heterogeneity in phytoplankton community composition during the 2008 North Atlantic Bloom Experiment. *Biogeosciences*, *12*(7), 2179–2194. https://doi.org/10.5194/bg-12-2179-2015

Chen, C.-C., Shiah, F.-K., Chung, S.-W., & Liu, K.-K. (2006). Winter phytoplankton blooms in the shallow mixed layer of the South China Sea enhanced by upwelling. *Journal of Marine Systems*, *59*(1-2), 97–110. https://doi.org/10.1016/j.jmarsys.2005.09.002

Claustre, H., Bishop, J., Boss, E., Bernard, S., Berthon, J.-F., Coatanoan, C., et al. (2010). Bio-optical profiling floats as new observational tools for biogeochemical and ecosystem studies: Potential synergies with ocean color remote sensing. In J. Hall, D. E. Harrison, & D. Stammer (Eds.), *"Proceedings of the OceanObs'09: Sustained Ocean Observations and Information for Society" Conference*. Venice, Italy: ESA Publ. WPP-306. https://doi.org/10.5270/OceanObs09.cwp.17

Coria-Monter, E., Monreal-Gómez, M. A., Salas-de-León, D. A., Aldeco-Ramírez, J., & Merino-Ibarra, M. (2014). Differential distribution of diatoms and dinoflagellates in a cyclonic eddy confined in the Bay of La Paz, Gulf of California. *Journal of Geophysical Research: Oceans*, *119*, 6258–6268. https://doi.org/10.1002/2014JC009916

Cullen, J. J. (1982). The deep chlorophyll maximum: Comparing vertical profiles of chlorophyll a. *Canadian Lournal of Fisheries and Aquatic Sciences*, *9*, 791–803.

Dall'Olmo, G., Westberry, T. K., Behrenfeld, M. J., Boss, E., & Slade, W. H. (2009). Significant contribution of large particles to optical backscattering in the open ocean. *Biogeosciences*, *6*(6), 947–967. https://doi.org/10.5194/bg-6-947-2009

Duan, R., Yang, K., Ma, Y., & Hu, T. (2012). A study of the mixed layer of the South China Sea based on the multiple linear regression. *Acta Oceanologica Sinica*, *31*(6), 19–31. https://doi.org/10.1007/s13131-012-0250-8

Dufois, F., Hardman-Mountford, N. J., Fernandes, M., Wojtasiewicz, B., Shenoy, D., Slawinski, D., et al. (2017). Observational insights into chlorophyll distributions of subtropical South Indian Ocean eddies. *Geophysical Research Letters*, *44*, 3255–3264. https://doi.org/10.1002/2016GL072371

Fennel, K., & Boss, E. (2003). Subsurface maxima of phytoplankton and chlorophyll: Steady-state solutions from a simple model. *Limnology and Oceanography*, *48*(4), 1521–1534. https://doi.org/10.4319/lo.2003.48.4.1521

Fukuzaki, K., Imai, I., Fukushima, K., Ishii, K.-I., Sawayama, S., & Yoshioka, T. (2014). Fluorescent characteristics of dissolved organic matter produced by bloom-forming coastal phytoplankton. *Journal of Plankton Research*, *36*(3), 685–694. https://doi.org/10.1093/plankt/fbu015

Gao, S., Wang, H., Liu, G., & Li, H. (2013). Spatio-temporal variability of chlorophyll a and its responses to sea surface temperature, winds and height anomaly in the western South China Sea. *Acta Oceanologica Sinica*, *32*(1), 48–58. https://doi.org/10.1007/s13131-013-0266-8

Geider, R. J., MacIntyre, H. L., & Kana, T. M. (1997). Dynamic model of phytoplankton growth and acclimation: Responses of the balanced growth rate and the chlorophyll a:carbon ratio to light, nutrient-limitation and temperature. *Marine Ecology Progress Series*, *148*, 187–200. https://doi.org/10.3354/meps148187

Gong, X., Jiang, W., Wang, L., Gao, H., Boss, E., Yao, X., et al. (2017). Analytical solution of the nitracline with the evolution of subsurface chlorophyll maximum in stratified water columns. *Biogeosciences*, *14*(9), 2371–2386. https://doi.org/10.5194/bg-14-2371-2017

Gong, X., Shi, J., & Gao, H. (2014). Modeling seasonal variations of subsurface chlorophyll maximum in South China Sea. *Journal of Ocean University of China*, *13*(4), 561–571. https://doi.org/10.1007/s11802-014-2060-4

Graff, J. R., Westberry, T. K., Milligan, A. J., Brown, M. B., Dall'Olmo, G., Dongen-Vogels, V. ., et al. (2015). Analytical phytoplankton carbon measurements spanning diverse ecosystems. *Deep Sea Research Part I: Oceanographic Research Papers*, *102*, 16–25. https://doi.org/10.1016/j.dsr.2015.04.006

Hu, J., Kawamura, H., Hong, H., & Qi, Y. (2000). A review on the currents in the South China Sea: Seasonal circulation, South China Sea Warm Current and Kuroshio intrusion. *Journal of Oceanography*, *56*(6), 607–624. https://doi.org/10.1023/A:1011117531252

Huang, B., Hu, J., Xu, H., Cao, Z., & Wang, D. (2010). Phytoplankton community at warm eddies in the northern South China Sea in winter 2003/2004. *Deep-Sea Research Part II: Topical Studies in Oceanography*, *57*(19-20), 1792–1798. https://doi.org/10.1016/j.dsr2.2010.04.005

Huot, Y., Morel, A., Twardowski, M. S., Stramski, D., & Reynolds, R. A. (2008). Particle optical backscattering along a chlorophyll gradient in the upper layer of the eastern South Pacific Ocean. *Biogeosciences*, *5*(2), 495–507. https://doi.org/10.5194/bg-5-495-2008

Kinsey, J. D., Corradino, G., Ziervogel, K., Schnetzer, A., & Osburn, C. L. (2018). Formation of chromophoric dissolved organic matter by bacterial degradation of phytoplankton-derived aggregates. *Frontiers in Marine Science*, *4*, 430. https://doi.org/10.3389/fmars.2017.00430

Kitchen, J. C., & Zaneveld, V. J. R. (1990). On the noncorrelation of the vertical structure of light scattering and chlorophyll α in case I waters. *Journal of Geophysical Research*, *95*(C11), 20,237–20,246. https://doi.org/10.1029/JC095iC11p20237

Lacour, L., Ardyna, M., Stec, K. F., Claustre, H., Prieur, L., Poteau, A., et al. (2017). Unexpected winter phytoplankton blooms in the North Atlantic subpolar gyre. *Nature Geoscience*, *10*(11), 836–839. https://doi.org/10.1038/ngeo3035

Lacour, L., Claustre, H., Prieur, L., & D'Ortenzio, F. (2015). Phytoplankton biomass cycles in the North Atlantic subpolar gyre: A similar mechanism for two different blooms in the Labrador Sea. *Geophysical Research Letters*, *42*, 5403–5410. https://doi.org/10.1002/2015GL064540

Laiolo, L., McInnes, A. S., Matear, R., & Doblin, M. A. (2016). Key drivers of seasonal plankton dynamics in cyclonic and anticyclonic eddies off east Australia. *Frontiers in Marine Science*, *3*, 155.

Letelier, R. M., Karl, D. M., Abbott, M. R., & Bidigare, R. R. (2004). Light driven seasonal patterns of chlorophyll and nitrate in the lower euphotic zone of the North Pacific Subtropical Gyre. *Limnology and Oceanography*, *49*(2), 508–519. https://doi.org/10.4319/lo.2004.49.2.0508

Liang, W., Tang, D., & Luo, X. (2018). Phytoplankton size structure in the western South China Sea under the influence of a "jet-eddy system". *Journal of Marine Systems*, *187*, 82–95. https://doi.org/10.1016/j.jmarsys.2018.07.001

Llort, J., Langlais, C., Matear, R., Moreau, S., Lenton, A., & Strutton, P. G. (2018). Evaluating Southern Ocean carbon eddy-pump from Biogeochemical-Argo floats. *Journal of Geophysical Research: Oceans*, *123*, 971–984. https://doi.org/10.1002/2017JC012861

Loisel, H., Bosc, E., Stramski, D., Oubelkheir, K., & Deschamps, P.-Y. (2001). Seasonal variability of the backscattering coefficient in the Mediterranean Sea on Satellite SeaWiFS imagery. *Geophysical Research Letters*, *28*(22), 4203–4206. https://doi.org/10.1029/2001GL013863

Lu, W., Yan, X.-H., & Jiang, Y. (2015). Winter bloom and associated upwelling northwest of the Luzon Island: A coupled physical-biological modeling approach. *Journal of Geophysical Research: Oceans*, *120*, 533–546. https://doi.org/10.1002/2014JC010218

Lu, Z., Gan, J., Dai, M., & Cheung, A. (2010). The influence of coastal upwelling and a river plume on the subsurface chlorophyll maximum over the shelf of the northeastern South China Sea. *Journal of Marine Systems*, *82*(1-2), 35–46. https://doi.org/10.1016/j.jmarsys.2010.03.002

McDougall, T., & Barker, P. (2011). Getting started with TEOS-10 and the Gibbs Seawater (GSW) oceanographic toolbox. SCOR/IAPSO, WG127, 28 pp.

McGillicuddy, D. (2016). Mechanisms of physical-biological-biogeochemical interaction at the oceanic mesoscale. *Annual Review of Marine Science*, *8*(1), 125–159. https://doi.org/10.1146/annurev-marine-010814-015606

Mignot, A., Claustre, H., Uitz, J., Poteau, A., D'Ortenzio, F., & Xing, X. (2014). Understanding the seasonal dynamics of phytoplankton biomass and the deep chlorophyll maximum in oligotrophic environments: A Bio-Argo float investigation. *Global Biogeochemical Cycles*, *28*, 856–876. https://doi.org/10.1002/2013GB004781

Mignot, A., Ferrari, R., & Claustre, H. (2018). Floats with bio-optical sensors reveal what processes trigger the North Atlantic bloom. *Nature Communications*, *9*(1), 190. https://doi.org/10.1038/s41467-017-02143-6

Morel, A. (1988). Optical modeling of the upper ocean in relation to its biogenous matter content (Case I waters). *Journal of Geophysical Research*, *93*(C9), 10,749–10,768. https://doi.org/10.1029/JC093iC09p10749

Morel, A., Huot, Y., Gentili, B., Werdell, P. J., Hooker, S. B., & Franz, B. A. (2007). Examining the consistency of products derived from various ocean color sensors in open ocean (Case 1) waters in the perspective of a multi-sensor approach. *Remote Sensing of Environment*, *111*(1), 69–88. https://doi.org/10.1016/j.rse.2007.03.012

Niewiadomska, K., Claustre, H., Prieur, L., & D'Ortenzio, F. (2008). Submesoscale physical-biogeochemical coupling across the Ligurian current (northwestern Mediterranean) using a bio-optical glider. *Limnology and Oceanography*, *53*(5), 2210–2225. https://doi.org/10.4319/lo.2008.53.5_part_2.2210

Ning, X., Chai, F., Xue, H., Cai, Y., Liu, C., & Shi, J. (2004). Physical-biological oceanographic coupling influencing phytoplankton and primary production in the South China Sea. *Journal of Geophysical Research*, *109*, C10005. https://doi.org/10.1029/2004JC002365

Peñaflor, E. L., Villanoy, C. L., Liu, C.-T., & David, L. T. (2007). Detection of monsoonal phytoplankton blooms in Luzon Strait with MODIS data. *Remote Sensing of Environment*, *109*(4), 443–450. https://doi.org/10.1016/j.rse.2007.01.019

Qu, T. (2001). Role of ocean dynamics in determining the mean seasonal cycle of the South China Sea surface temperature. *Journal of Geophysical Research*, *106*(C4), 6943–6955. https://doi.org/10.1029/2000JC000479

Qu, T., Du, Y., Gan, J., & Wang, D. (2007). Mean seasonal cycle of isothermal depth in the South China Sea. *Journal of Geophysical Research*, *112*, C02020. https://doi.org/10.1029/2006JC003583

Ras, J., Claustre, H., & Uitz, J. (2008). Spatial variability of phytoplankton pigment distributions in the Subtropical South Pacific Ocean: Comparison between in situ and predicted data. *Biogeosciences*, *5*(2), 353–369. https://doi.org/10.5194/bg-5-353-2008

Rochelle-Newall, E. J., & Fisher, T. R. (2002). Production of chromophoric dissolved organic matter fluorescence in marine and estuarine environments: An investigation into the role of phytoplankton. *Marine Chemistry*, *77*(1), 7–21. https://doi.org/10.1016/S0304-4203(01)00072-X

Sauzède, R., Claustre, H., Pasqueron de Fommervault, O., Bittig, H., Gattuso, J.-P., Legendre, L., & Johnson, K. S. (2017). Global estimates of water column nutrients concentration and carbonate system parameters in the Ocean: A novel approach based on neural networks. *Frontiers in Marine Science*, *4*, 128. https://doi.org/10.3389/fmars.2017.00128

Shang, S., Li, L., Li, J., Li, Y., Lin, G., & Sun, J. (2012). Phytoplankton bloom during the northeast monsoon in the Luzon Strait bordering the Kuroshio. *Remote Sensing of Environment*, *124*, 38–48. https://doi.org/10.1016/j.rse.2012.04.022

Shen, S., Leptoukh, G. G., Acker, J. G., Yu, Z., & Kempler, S. J. (2008). Seasonal variations of chlorophyll a concentration in the northern South China Sea. *IEEE Geoscience and Remote Sensing Letters*, *5*(2), 315–319. https://doi.org/10.1109/LGRS.2008.915932

Siegel, D. A., Behrenfeld, M. J., Maritorena, S., McClain, C. R., Antoine, D., Bailey, S. W., et al. (2013). Regional to global assessments of phytoplankton dynamics from the SeaWiFS mission. *Remote Sensing of Environment*, *135*, 77–91. https://doi.org/10.1016/j.rse.2013.03.025

Siegel, D. A., Maritorena, S., Nelson, N. B., & Behrenfeld, M. J. (2005). Independence and interdependencies among global ocean color properties: Reassessing the bio-optical assumption. *Journal of Geophysical Research*, *110*, C07011. https://doi.org/10.1029/2004JC002527

Stramski, D., Boss, E., Bogucki, D., & Voss, K. J. (2004). The role of seawater constituents in light backscattering in the ocean. *Progress in Oceanography*, *61*(1), 27–56. https://doi.org/10.1016/j.pocean.2004.07.001

Tang, D. L., Ni, I. H., Kester, D. R., & Müller-Karger, F. E. (1999). Remote sensing observations of winter phytoplankton blooms southwest of the Luzon Strait in the South China Sea. *Marine Ecology Progress Series*, *191*, 43–51. https://doi.org/10.3354/meps191043

Thomalla, S. J., Ogunkoya, A. G., Vichi, M., & Swart, S. (2017). Using optical sensors on gliders to estimate phytoplankton carbon concentrations and chlorophyll-to-carbon ratios in the Southern Ocean. *Frontiers in Marine Science*, *4*, 34. https://doi.org/10.3389/fmars.2017.00034

Twardowski, M. S., Boss, E., Macdonald, J. B., Pegau, W. S., Barnard, A. H., & Zaneveld, J. R. V. (2001). A model for estimating bulk refractive index from the optical backscattering ratio and the implications for understanding particle composition in Case I and Case II waters. *Journal of Geophysical Research*, *106*(C7), 14,129–14,142. https://doi.org/10.1029/2000JC000404

Vaillancourt, R. D., Marra, J., Seki, M. P., & Bidigare, R. R. (2003). Impact of a cyclonic eddy on phytoplankton community structure and photosynthetic competency in the subtropical North Pacific Ocean. *Deep-Sea Research Part I: Oceanographic Research Papers*, *50*(7), 829–847. https://doi.org/10.1016/S0967-0637(03)00059-1

Wang, J. J., Tang, D. L., & Sui, Y. (2010). Winter phytoplankton bloom induced by subsurface upwelling and mixed layer entrainment southwest of Luzon Strait. *Journal of Marine Systems*, *83*(3-4), 141–149. https://doi.org/10.1016/j.jmarsys.2010.05.006

Westberry, T. K., Dall'Olmo, G., Boss, E., Behrenfeld, M. J., & Moutin, T. (2010). Coherence of particulate beam attenuation and backscattering coefficients in diverse open ocean environments. *Optics Express*, *18*(15), 15,419–15,425. https://doi.org/10.1364/OE.18.015419

Whitmire, A. L., Letelier, R. M., Villagrán, V., & Ulloa, O. (2009). Autonomous observations of in vivo fluorescence and particle backscattering in an oceanic oxygen minimum zone. *Optics Express*, *17*(24), 21,992–22,004. https://doi.org/10.1364/OE.17.021992

Winkler, L. W. (1888). Die Bestimmung des im Wasser gelösten Sauerstoffes. *Berichte der Deutschen Chemischen Gesellschaft*, *21*(2), 2843–2854. https://doi.org/10.1002/cber.188802102122

Wong, G. T. F., Ku, T.-L., Mulholland, M., Tseng, C.-M., & Wang, D.-P. (2007). The SouthEast Asian time-series study (SEATS) and the biogeochemistry of the South China Sea—An overview. *Deep-Sea Research Part II: Topical Studies in Oceanography*, *54*(14-15), 1434–1447. https://doi.org/10.1016/j.dsr2.2007.05.012

Xiao, W., Wang, L., Laws, E., Xie, Y., Chen, J., Liu, X., et al. (2018). Realized niches explain spatial gradients in seasonal abundance of phytoplankton groups in the South China Sea. *Progress in Oceanography*, *162*, 223–239. https://doi.org/10.1016/j.pocean.2018.03.008

Xing, X., Claustre, H., Uitz, J., Mignot, A., Poteau, A., & Wang, H. (2014). Seasonal variations of bio-optical properties and their interrelationships observed by Bio-Argo floats in the subpolar North Atlantic. *Journal of Geophysical Research: Oceans*, *119*, 7372–7388. https://doi.org/10.1002/2014JC010189

Xing, X., Claustre, H., Wang, H., Poteau, A., & D'Ortenzio, F. (2014). Seasonal dynamics in colored dissolved organic matter in the Mediterranean Sea: Patterns and drivers. *Deep-Sea Research Part I: Oceanographic Research Papers*, *83*, 93–101. https://doi.org/10.1016/j.dsr.2013.09.008

Xing, X., Morel, A., Claustre, H., D'Ortenzio, F., & Poteau, A. (2012). Combined processing and mutual interpretation of radiometry and fluorometry from autonomous profiling Bio-Argo floats: 2. Colored dissolved organic matter absorption retrieval. *Journal of Geophysical Research*, *117*, C04022. https://doi.org/10.1029/2011JC007632

Xiu, P., & Chai, F. (2011). Modeled biogeochemical responses to mesoscale eddies in the South China Sea. *Journal of Geophysical Research*, *116*, C10006. https://doi.org/10.1029/2010JC006800

Xue, H., Chai, F., Pettigrew, N., Xu, D., Shi, M., & Xu, J. (2004). Kuroshio intrusion and the circulation in the South China Sea. *Journal of Geophysical Research*, *109*, C02017. https://doi.org/10.1029/2002JC001724

Zhang, W.-Z., Wang, H., Chai, F., & Qiu, G. (2016). Physical drivers of chlorophyll variability in the open South China Sea. *Journal of Geophysical Research: Oceans*, *121*, 7123–7140. https://doi.org/10.1002/2016JC011983